ACSNANO
www.acsnano.org

ARTICLE

High-Performance WSe_2 Field-Effect Transistors *via* Controlled Formation of In-Plane Heterojunctions

Bilu Liu,[†] Yuqiang Ma,[†] Anyi Zhang, Liang Chen, Ahmad N. Abbas, Yihang Liu, Chenfei Shen, Haochuan Wan, and Chongwu Zhou*

Ming Hsieh Department of Electrical Engineering, University of Southern California, Los Angeles, California 90089, United States

Supporting Information

ABSTRACT: **Monolayer WSe_2 is a two-dimensional (2D) semiconductor with a direct band gap, and it has been recently explored as a promising material for electronics and optoelectronics. Low field-effect mobility is the main constraint preventing WSe_2 from becoming one of the competing channel materials for field-effect transistors (FETs). Recent results have demonstrated that chemical treatments can modify the electrical properties of transition metal dichalcogenides (TMDCs), including MoS_2 and WSe_2. Here, we report that controlled heating in air significantly improves device performance of WSe_2 FETs in terms of on-state currents and field-effect mobilities. Specifically, after being heated at optimized conditions, chemical vapor deposition grown monolayer WSe_2 FETs showed an average FET mobility of 31 $cm^2 \cdot V^{-1} \cdot s^{-1}$ and on/off current ratios up to 5×10^8. For few-layer WSe_2 FETs, after the same treatment applied, we achieved a high mobility up to 92 $cm^2 \cdot V^{-1} \cdot s^{-1}$. These values are significantly higher than FETs fabricated using as-grown WSe_2 flakes without heating treatment, demonstrating the effectiveness of air heating on the performance improvements of WSe_2 FETs. The underlying chemical processes involved during air heating and the formation of in-plane heterojunctions of WSe_2 and WO_{3-x}, which is believed to be the reason for the improved FET performance, were studied by spectroscopy and transmission electron microscopy. We further demonstrated that, by combining the air heating method developed in this work with supporting 2D materials on the BN substrate, we achieved a noteworthy field-effect mobility of 83 $cm^2 \cdot V^{-1} \cdot s^{-1}$ for monolayer WSe_2 FETs. This work is a step toward controlled modification of the properties of WSe_2 and potentially other TMDCs and may greatly improve device performance for future applications of 2D materials in electronics and optoelectronics.**

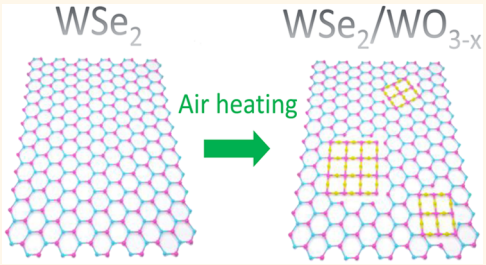

KEYWORDS: *two-dimensional materials, tungsten diselenide, WSe_2, tungsten oxide, heterojunctions, field-effect transistor, mobility*

Two dimensional (2D) semiconducting transition metal dichalcogenides (TMDCs) have ignited substantial scientific interest in the past few years due to their unique structures and properties, which satisfy the requirements of many electronic devices. One of the primary advantages of field-effect transistors (FETs) based on atomically thin TMDCs is the absence of dangling bonds on the top and bottom surfaces of these materials, which prevents performance degradation of the devices due to interface states.[1−4] In addition, the ultrathin body of TMDCs can result in a strong electrostatic gating of these materials, making them attractive for electronics and optoelectronics.[5] Another advantage for TMDCs is that by tuning compositions, number of layers, and strains, scientists can modify the electronic properties of these materials.[6−15] Accordingly, direct or indirect band gap materials and n-type, p-type, or ambipolar FET devices have been fabricated.[2,8,15−20] The enhanced spin−orbit coupling in TMDCs also makes it possible to use spin and valley information on carriers for various kinds of devices.[21] Meanwhile, investigations of monolayer TMDCs have also indicated profound physics like many-body quasiparticles, including trions and biexcitons, which have no analogue in bulk semiconductors.[22] Due to these extraordinary merits, devices fabricated from either mechanically exfoliated or vapor-phase-grown TMDCs have been proven to show interesting electronic, optical, catalytic, and energy storage properties.[2,13,17,23,24] Among all TMDCs, semiconducting MoS_2 is the one which has received the most attention, while research interest in WSe_2 has shown rapid increase recently.[4,13] Compared with monolayer MoS_2, monolayer WSe_2 possesses a smaller band gap (~1.6 eV in monolayer WSe_2 and ~1.8 eV in monolayer MoS_2), and on average, the field-effect mobilities are higher in WSe_2 FETs than in MoS_2 FETs. Recent experiments have also showed that both n-type FETs,[18] p-

Received: January 22, 2016
Accepted: May 5, 2016

DOI: 10.1021/acsnano.6b00527
ACS Nano XXXX, XXX, XXX−XXX

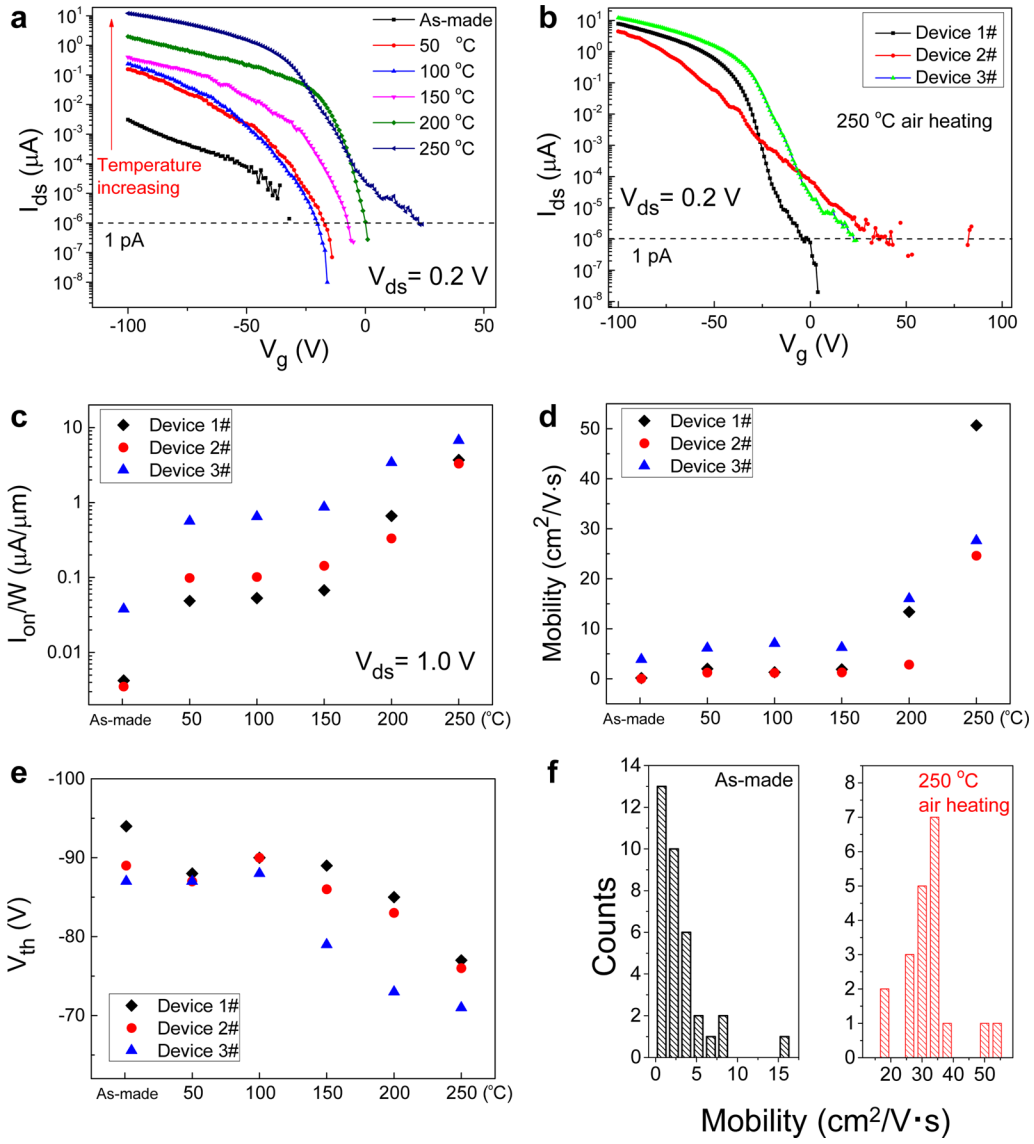

Figure 1. Improved FET performance of CVD-grown monolayer WSe_2 *via* controlled heating in air. (a) I_{ds}−V_g curves of a representative monolayer WSe_2 FET in an as-made state as well as after air heating at different temperatures. (b) I_{ds}−V_g curves of three WSe_2 transistors after 250 °C air heating. Changes of I_{on}/W (c), field-effect mobility (d), and V_{th} (e) *versus* heating temperatures for three devices shown in (b). (f) Mobility distributions of monolayer WSe_2 FETs in the as-made state and the same devices after 250 °C air heating.

type FETs,[16] as well as complementary inverters[17] were fabricated based on WSe_2, which has been proven to be difficult in MoS_2 due to Fermi level pinning effects. Therefore, from the aforementioned comparisons, WSe_2 appears promising for future FET applications.

Because of a large amount of surface atoms, TMDCs and other 2D materials have been shown to be very susceptible to environments.[25−28] This feature benefits their applications in chemical and biomedicine sensing but, on the other hand, raises a crucial concern about the stability of TMDC devices. Recent results have indicated that TMDCs can be oxidized at moderate temperatures in oxygen or ozone environments, leading to the formation of metal oxides which have distinct electronic properties with TMDC themselves.[29−32] Therefore, the stability of TMDC devices in ambient air is of particular importance concerning the practical use of these materials. Moreover, recent reports also indicate that properties of TMDCs are tunable, by means of chemical treatments such as ion intercalation. These facts also make it interesting to explore whether we can take advantages of such treatments to modify the properties of TMDCs and further to improve their FET performance because low mobility is one of the key limiting factors that hinder applications of TDMC FETs currently. In this work, we demonstrated such a simple yet effective air heating method which significantly improves device performance of WSe_2 FETs *via* controlled formation of in-plane heterojunctions of WSe_2 and WO_{3-x}.

RESULTS AND DISCUSSION

We first show the effectiveness of air heating in improving FET performance of chemical vapor deposition (CVD)-grown monolayer WSe_2. The CVD-grown WSe_2 flakes used in these experiments were synthesized at 950 °C and were monolayers, as revealed by atomic force microscopy (AFM), Raman, and photoluminescence (PL) spectroscopy characterization (Supporting Information Figure S1). As mentioned above, monolayer materials are very susceptible to their environments,

DOI: 10.1021/acsnano.6b00527
ACS Nano XXXX, XXX, XXX−XXX

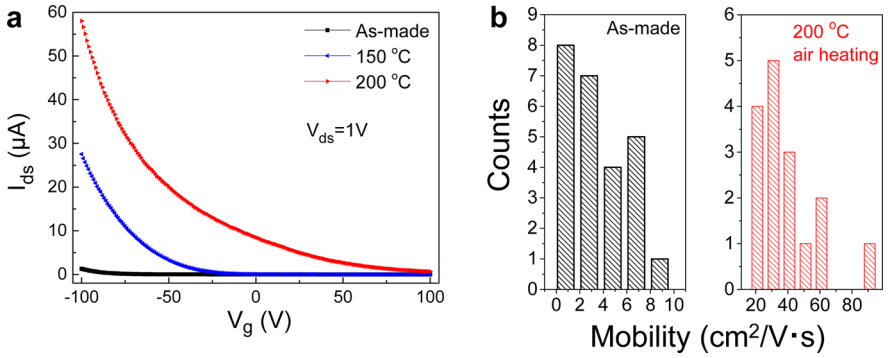

Figure 2. Improved FET performance of PVD-grown few-layer WSe_2 FETs *via* controlled heating in air. (a) I_{ds}–V_g curves of a representative few-layer WSe_2 devices at different conditions. (b) Field-effect mobility distributions of few-layer WSe_2 FETs in as-made state and after 200 °C air heating.

which may have nontrivial influences on their electronic properties. Surprisingly, we found that the on-state current of back-gated monolayer WSe_2 FETs increased by 8-fold, field-effect mobility increased by 5-fold, and current on/off ratios increased by 10-fold, after leaving the device in ambient air at room temperature for an extended duration of 9 months (Figure S2). This phenomenon (*i.e.*, improved FET performance after leaving devices in air) was observed for all the devices (>30) we fabricated, showing that the results were highly reproducible. Then an important question raised is whether this process could be accelerated by certain means. It is quite rational to think of raising the temperature while leaving the devices in air, that is, heating the WSe_2 FETs in air at elevated temperatures. We have conducted systematic studies of air heating on several WSe_2 FETs under different heating temperatures to find the optimal temperature. Figure 1a shows the transfer characteristics (I_{ds}–V_g) of a typical monolayer WSe_2 FET in as-fabricated form, as well as after heating in air at 50, 100, 150, 200, and 250 °C. As can be clearly discerned, the on-state currents continued to increase when the FET was sequentially heated and reached a maximum of 12 μA after 250 °C. Noticeably, compared to the as-fabricated FET, the on-current of the FET heated at 250 °C increased by 4000 times. Figure 1b shows I_{ds}–V_g curves in a semilog scale of three typical devices after 250 °C air heating, all possessing high on/off ratios above 10^7, which are significantly greater than the as-fabricated FETs. At different heating temperatures, these devices exhibited a substantial increase in the normalized on-state current (I_{on}/W, where W is the channel width of FETs), as shown in Figure 1c. All of them exhibited a maximum on-state current after 250 °C air heating. For the monolayer WSe_2 FETs heated in air at 300 °C, we found that the on-state currents significantly decreased (Supporting Information Figure S3). After further heating to 400 °C, all devices behaved as open circuits with noise level current and showed no gate dependence. The field-effect mobility *versus* heating conditions of these devices showed very similar trends with that of the on-current; that is, the FETs possess maximum field-effect mobilities after 250 °C air heating (Figure 1d). Additionally, we observed that the subthreshold voltage (V_{th}) of these devices gradually shifted to more positive voltages as the air temperature increased (Figure 1e). We note that all the measured FETs show a low off-state current of ~1 pA, and high current on/off ratios up to 5×10^8 were obtained. Figure 1f shows the field-effect mobility statistics of as-fabricated monolayer WSe_2 FETs and the same set of devices after heating in air at the optimized temperature of 250 °C. Noticeably, the maximum room temperature field-effect mobility reaches 51 $cm^2/V{\cdot}s$ for the air-heated monolayer WSe_2 FETs. After 250 °C air treatment, the average effective mobility of the CVD-grown monolayer WSe_2 is 31 $cm^2/V{\cdot}s$, which compares favorably to recent reports of monolayer TMDC-based FETs.[8,33−35] We also noted that these air-heated devices show relatively small variations of mobility, compared to other recent results.[35,36] Moreover, we found that after being heated in air at elevated temperatures, the WSe_2 FETs became very stable, and we did not observe any noticeable change in device characteristics when leaving them in ambient air at room temperature for months. This result suggests that, besides the improved FET performance, air heating at high temperatures can also suppress the environmental susceptibility of WSe_2 devices at normal room temperature.

To examine the generality of the above air heating method in improving device performance of WSe_2 FETs, we have further applied this method to transistors made of few-layer WSe_2 flakes, and we demonstrated that the same method also worked for few-layer WSe_2 FETs. The few-layer WSe_2 samples were grown by a physical vapor deposition (PVD) method using WSe_2 powders as source materials (see Methods section for the details of the PVD growth and Supporting Information Figure S4 for the characterization of PVD-grown WSe_2 samples). Figure 2a shows I_{ds}–V_g curves of a typical few-layer WSe_2 FET in the as-fabricated state and after air heating at 150 and 200 °C. As can be clearly seen, similar improvement of on-state current after device heating in air was observed. This observation suggests the generality of the developed air heating method above in improving device performance of both monolayer and few-layer WSe_2 samples grown by different methods. The field-effect mobility distributions of as-fabricated few-layer WSe_2 FETs and the devices after heating in air at 200 °C are plotted in Figure 2b. Again, one can see that the air-heated few-layer WSe_2 FETs possess mobilities much higher than those of the as-fabricated FETs, with a maximum mobility of 92 $cm^2/V{\cdot}s$. We noted that for few-layer WSe_2, the optimized heating temperature is 200 °C. After further increasing the temperature to 250 °C, even though the on-state current kept increasing, the on/off ratios dropped significantly for few-layer WSe_2 FETs (Supporting Information Figure S5). The reason for such different behaviors between monolayer and few-layer WSe_2 FETs will be discussed later.

It is important to understand what happened during air heating and the mechanism behind the improvement of device

DOI: 10.1021/acsnano.6b00527
ACS Nano XXXX, XXX, XXX−XXX

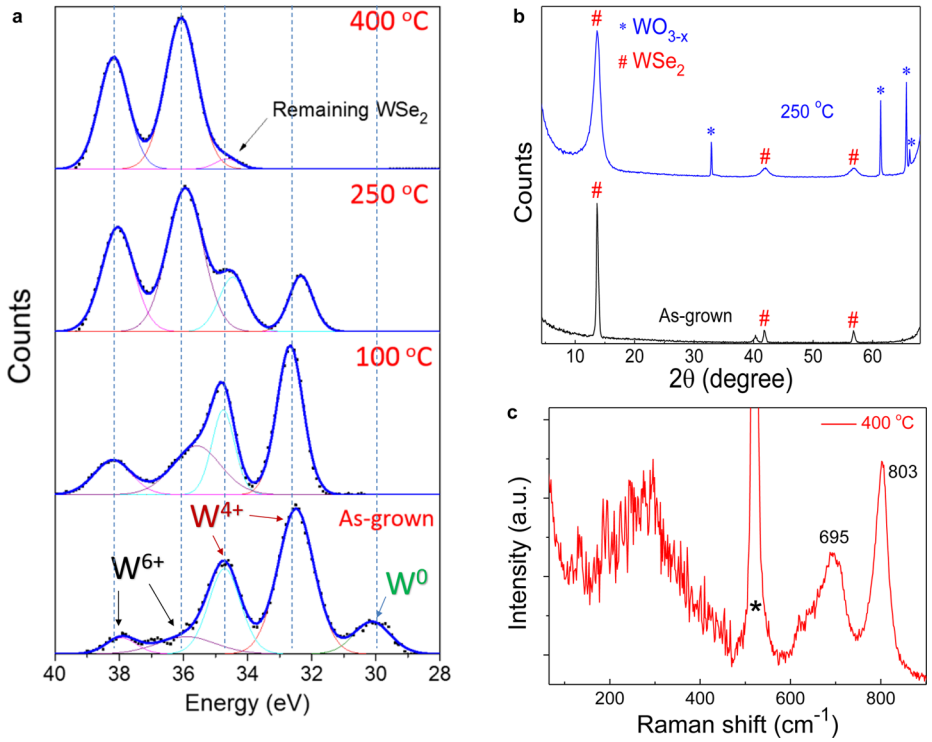

Figure 3. Spectroscopy studies of WSe_2 samples. (a) XPS spectra of the as-grown few-layer WSe_2 sample and the same sample after air heating at different temperatures. Note that the intensity ratios of W^{6+}/W^{4+} increase with increasing heating temperatures. (b) XRD patterns of as-grown few-layer WSe_2 and the same sample after 250 °C air heating. (c) Raman spectra of the PVD few-layer WSe_2 sample after air heating at 400 °C. The two peaks at 695 and 803 cm^{-1} can be assigned to tungsten oxide. The peak with a star (*) at 520 cm^{-1} indicates the characteristic peak of the Si substrate.

performance for WSe_2 FETs heated in air. To study the chemistry involved during the air heating process, we performed both macro- and microscale characterization to investigate the structures and properties of as-prepared and air-heated WSe_2 samples. For these experiments, we used PVD-grown few-layer WSe_2 since PVD synthesis does not require the use of WO_3 as a precursor during WSe_2 growth (see Methods), which can exclude the influence of oxide in source materials in subsequent spectroscopy analysis. X-ray photoemission spectroscopy (XPS) measurements on as-prepared WSe_2 show two major peaks at ~34.7 and 32.5 eV, corresponding to the W^{4+} $4f_{5/2}$ and W^{4+} $4f_{7/2}$ in WSe_2, respectively.[32,37] A small peak at 30.1 eV was also observed, corresponding to pure W, which may be a decomposition product of the WSe_2 precursor. Small peaks at ~38.2 and 36.1 eV, which can be assigned to W^{6+} $4f_{5/2}$ and W^{6+} $4f_{7/2}$ in WO_3,[37] were also observed. The existence of weak oxide peaks in as-grown PVD WSe_2 may be due to air exposure of the samples before loading them into the XPS chamber. Noticeably, one can see that as the air heating temperature increases, the intensity ratios of W^{6+}/W^{4+} keep increasing. These results indicate gradual incorporation of oxygen into WSe_2 and the formation of WO_3 after air heating. We also conducted X-ray diffraction (XRD, Figure 3b) measurements on as-grown and air-heated WSe_2 samples. The appearance of diffraction peaks at 32.9, 61.4, 65.6, and 66.3° suggests the formation of WO_3, in good accordance with the XPS results in Figure 3a. Observations from micro-Raman performed on air-heated WSe_2 flakes again show the formation of tungsten oxides at 695 and 803 cm^{-1} (Figure 3c), which are very close to the Raman peaks of WO_3. Certain red shifts for both peaks can be caused by the existence of oxygen deficiency, that is, the formation of the nonstoichiometric WO_{3-x} oxidized species.[38] Collectively, the above XPS, XRD, and Raman spectroscopic results suggest the formation of WO_{3-x} in air-heated WSe_2 flakes, which is consistent with recent studies on the oxidation of MoS_2 and WSe_2 flakes.[30,39]

We also performed high-resolution transmission electron microscopy (HRTEM) studies on the air-heated WSe_2 and found the formation of in-plane heterojunctions of WSe_2 and WO_{3-x} in air-heated WSe_2 flakes (Figure 4a–d). From the fast Fourier transforms (FFTs, Figure 4b,c) of the selected regions in Figure 4a, one can clearly identify both hexagonal WSe_2 as well as cubic WO_{3-x} phases. Figure 4d clearly shows the interface between WSe_2 and WO_{3-x} domains. The two phases form so-called quilted in-plane heterostructures, as schematically shown in Figure 4e. The sizes of the newly formed cubic WO_{3-x} domains are in the range of a few to a few tens of nanometers. This kind of quilted heterostructure was also found in liquid-exfoliated MoS_2 flakes very recently.[40]

Now the question becomes how the formation of WSe_2/WO_{3-x} in-plane heterojunctions improved device performance of WSe_2 FETs. We speculate that there are two effects that may be responsible for the improved device performance of air-heated WSe_2 FETs. First, it has been well-documented that nonstoichiometric tungsten oxide (WO_{3-x}) is a highly conductive species. For example, Liu *et al.* showed that partial oxidation of WSe_2 resulted in the formation of WO_{3-x}, which is highly conductive with a sheet resistance of ~10^5 ohm/sq, while WSe_2 possess a 3 orders of magnitude higher sheet resistance of ~10^8 ohm/sq.[30] Therefore, the effective channel lengths of FETs would be reduced *via* the formation of highly conductive WO_{3-x} domains in WSe_2. This will in turn result in

DOI: 10.1021/acsnano.6b00527
ACS Nano XXXX, XXX, XXX–XXX

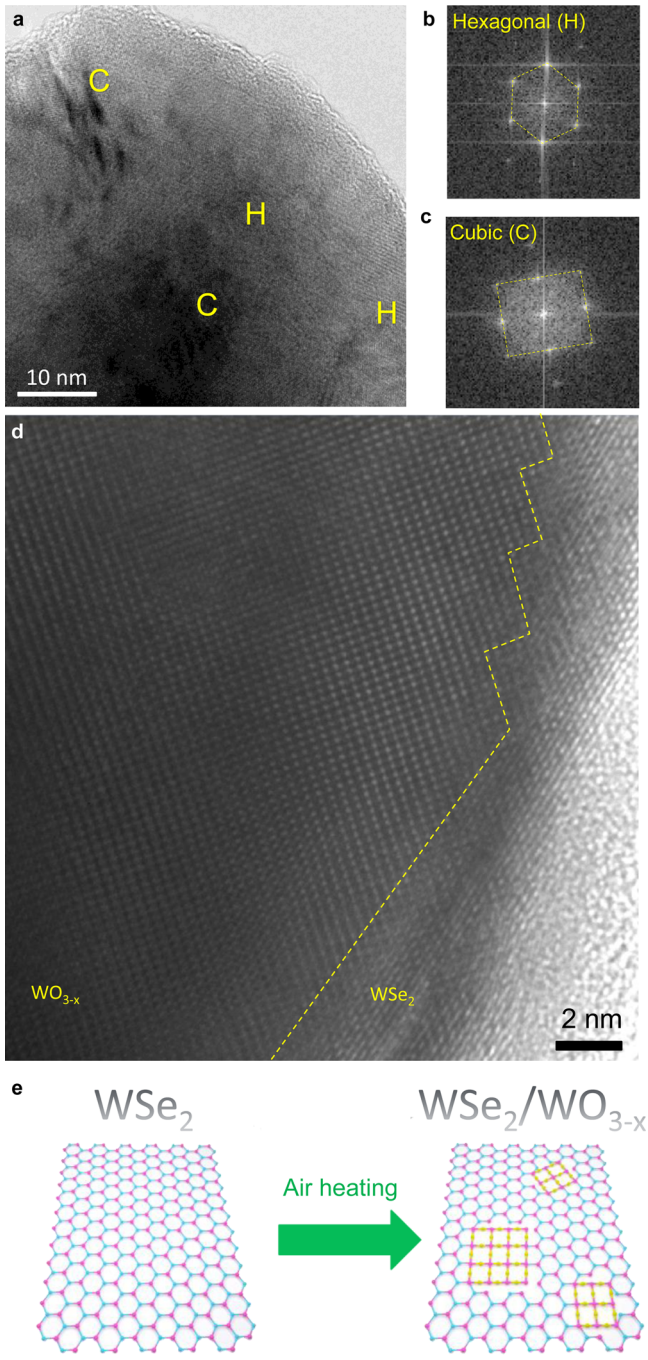

Figure 4. TEM characterization and schematics of in-plane heterojunctions of WO_{3-x} (cubic) and WSe_2 (hexagonal). (a) Typical TEM image of the WSe_2 sample after 150 °C air heating. Letter C stands for cubic, and letter H stands for hexgonal. (b) FFT taken at the letter H position, showing a hexagonal WSe_2 lattice. (c) FFT taken at the letter C position, showing the cubic WO_{3-x} lattice. (d) HRTEM image showing the interface (yellow dashed lines) between WO_{3-x} and WSe_2 domains. (e) Schematics of structural change during oxidation of WSe_2 during air heating, showing the formation of in-plane quilted heterostructures made of WSe_2 and WO_{3-x}.

an increase of device on-state current and field-effect mobility. Second, due to the work function mismatch between WSe_2 and WO_{3-x}, WO_{3-x} can dope WSe_2 in a p-type manner and increase hole concentrations in the device, which could increase the on-state current of p-type FETs, as well. Indeed, WO_{3-x} has been frequently used as a hole injection material in organic light emission devices, and p-type doping of WSe_2 by WO_{3-x} has been recently reported by Tsukagoshi's group.[32] In addition, such p-type doping of WSe_2 by WO_{3-x} would lead to a change of V_{th} of FETs toward more positive voltages, consistent with the experimental results shown in Figure 1e. Since WSe_2 and WO_{3-x} have different crystal structures and lattice constants, in-plane strain would be introduced during the WSe_2 to WO_{3-x} conversion process. The lattice mismatch may result in local physical gaps between WSe_2 and WO_{3-x} domains at some points. This situation happens only at high enough temperatures when a sufficient amount of WO_{3-x} domains are formed and comparable to WSe_2 domains. In this case, on-state currents for FETs based on monolayer WSe_2 will drop dramatically (as shown in Supporting Information Figure S3), and eventually, the devices can end up with open circuits. However, for multilayer WSe_2 flakes, the situation is a bit different as they are more tolerant to the in-plane cracking since the devices can still be conductive due to charge transport in the vertical direction, in addition to the in-plane transport. Therefore, this would lead to highly conductive thick WSe_2 flakes after air heating at elevated temperatures, consistent with our experiments (Supporting Information Figure S5). We also performed control experiments by heating WSe_2 FETs in vacuum, but we did not observe significant change in the device on-state current (Figure S6). This experiment confirms that heating-induced removal of surface impurities on WSe_2 does not play an important role in improving WSe_2 device performance upon air heating.

The performance of the WSe_2 FET can be further enhanced by combining the oxidation method developed in this work with other well-documented methods, for example, supporting 2D materials on flat and inert BN substrates. As an excellent dielectric material, BN has been reported to have the capability of providing dielectric interfaces with very little charge impurities to graphene, TMDCs, and other 2D materials. The schematic of a back-gated FET using WSe_2 on BN is shown in Figure 5a. First, we exfoliated BN flakes on Si/SiO_2 substrates using scotch tape. Then, monolayer WSe_2 flakes were grown directly on BN using the CVD method described above. PL spectrum confirmed that this WSe_2 flake on BN is a monolayer (Figure 5b). The successful growth of monolayer WSe_2 on BN flakes allows us to fabricate FETs based on this kind of vertical heterostructure. The height of the exfoliated BN layer was measured by AFM to be 317 nm (Supporting Information Figure S7). From the transfer characteristics, again we observed improvement of on-state current and field-effect mobility after 250 °C air heating of WSe_2 FET on BN substrates (Figure 5c,d). Notably, this monolayer WSe_2 device showed a room temperature mobility of 83 $cm^2 \cdot V^{-1} \cdot s^{-1}$, which is much higher than that of devices on Si/SiO_2 substrates (Figure 1). The output characteristics ($V_{ds}-I_{ds}$) and $V_{ds}-I_g$ family curves are shown in Figure 5e,f, showing a nice transistor behavior of FETs made from WSe_2 supported on BN substrates. These results suggest that the oxidation method can be combined with other fabrication techniques to enhance the mobility of WSe_2 FETs even further.

CONCLUSIONS

In conclusion, we have demonstrated that air heating of WSe_2 FETs resulted in a significantly improved device performance *via* the formation of in-plane heterojunctions of WSe_2 and their oxidation species WO_{3-x}, which is highly conductive. After

DOI: 10.1021/acsnano.6b00527
ACS Nano XXXX, XXX, XXX−XXX

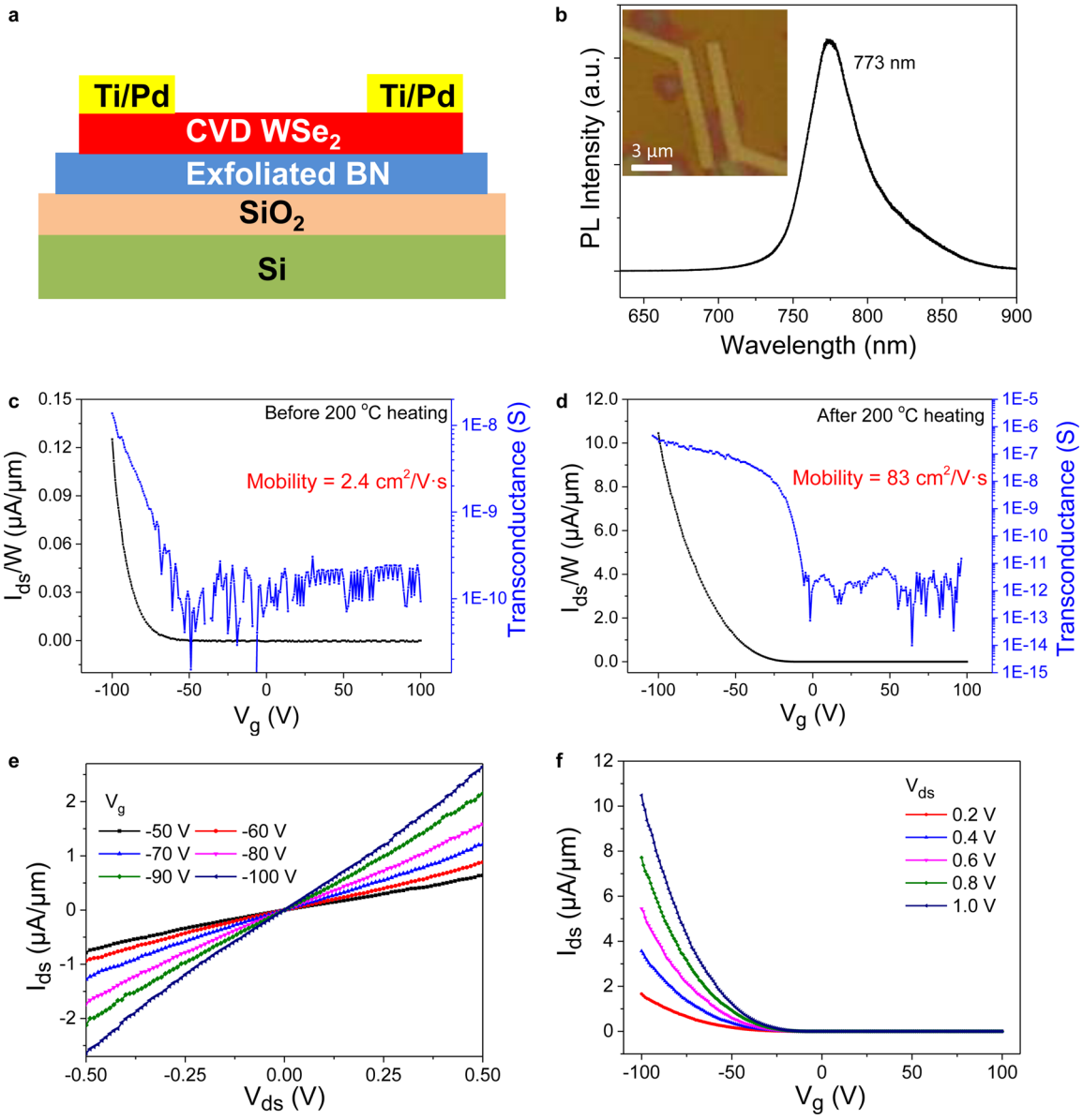

Figure 5. WSe_2 on BN devices. (a) Schematic of a FET based on WSe_2 grown on BN. (b) PL spectrum of the monolayer WSe_2 grown on BN. Inset shows an optical image of a FET device with WSe_2 on BN flake. (c,d) I_{ds}–V_g curves of the device shown in (b) before and after air heating at 200 °C. (e,f) I_{ds}–V_{ds} and I_{ds}–V_g family curves of the device shown in (b) after air heating at 200 °C.

optimized heating at 250 °C, the CVD monolayer WSe_2 transistors showed a maximum hole mobility of 51 $cm^2/V{\cdot}s$, an average mobility of 31 $cm^2/V{\cdot}s$, and device on/off ratio of 5×10^8. We further showed that the same method also works for PVD-grown few-layer WSe_2 transistors, demonstrating the generality of the air heating method to improve the FET performance of WSe_2. Spectroscopic and TEM characterization showed the formation of WO_{3-x} after air heating, which forms in-plane quilted heterostructures with the WSe_2 matrix and in turn resulted in an improved transistor performance of p-type WSe_2. We also demonstrated that combinations of the oxidation method developed in this work with supporting WSe_2 flakes on BN substrates further pushed the device performance to a higher level. Our results suggest that controlled oxidation may become a general approach for enhancing the performance of FETs made of WSe_2 and potentially many other TDMCs.

METHODS

CVD Growth of Monolayer WSe_2 Flakes. WO_3 (260 mg, 99.9%, Sigma-Aldrich) and Se (440 mg, 99.5%, Sigma-Aldrich) powders were used as tungsten and selenium sources for CVD growth of monolayer WSe_2, as reported in our previous work.[19] A three-zone furnace was used where Se powders were put in the first zone, and WO_3 powders were put in the third zone. The distance between the two sources was 55 cm. The temperatures of WO_3 and Se were 950 and 540 °C, respectively. The growth substrates were Si/SiO_2 (300 nm), and WSe_2 growth was conducted at 950 °C under ambient pressure and Ar/H_2 flow rates of 320/20 sccm for 15 min. After growth, the furnace was cooled to room temperature naturally under protection of Ar/H_2 (320/20 sccm).

For the growth of monolayer WSe_2 on BN, we first exfoliated BN flakes on Si/SiO_2 substrates using scotch tape. After the BN flakes were cleaned, the substrates were loaded into the three-zone furnace mentioned above. Then the growth of WSe_2 was conducted at 950 °C under ambient pressure and Ar/H_2 flow rates of 200/20 sccm for 20

DOI: 10.1021/acsnano.6b00527
ACS Nano XXXX, XXX, XXX–XXX

min. We found that the growth of WSe_2 was slower and growth yield was lower on BN substrates than direct growth on Si/SiO_2 substrates.

PVD Growth of Few-Layer WSe_2 Flakes. WSe_2 powders were used as the source material for the PVD synthesis of few-layer WSe_2 flakes. The growth temperature was 900 °C, and the pressure was 700 mTorr during the PVD growth process. A small amount of Ar (10 sccm) was introduced during growth, and the growth lasted for 15 min.

Material Characterization. The thickness and layer numbers of CVD- and PVD-grown WSe_2 flakes were evaluated using AFM (Dimensional 3100, Digital Instrument, tapping mode), Raman spectroscopy, and PL spectroscopy (Renishaw Raman with a 532 nm excitation laser and a laser spot size of ~1 μm). The air-heated WSe_2 flakes were characterized using Raman, XPS (The Kratos Axis Ultra DLD surface analysis instrument using focused monochromatized Al Kα radiation), XRD (Rigaku Ultima IV powder/thin-film diffractometer with Cu Kα line), and TEM (JEOL 2100F, 200 kV).

Device Fabrication and Measurements. E-beam lithography was used to fabricate back-gate WSe_2 devices. A bilayer PMMA e-beam resist was spin-coated on substrates, and EBL was conducted to define the source and drain electrodes. Ti/Pd (0.5 nm/50 nm) was deposited as source and drain contacts, and a bottom silicon substrate served as a global back gate. The device measurements were conducted in ambient conditions using an Agilent 4156B semiconductor parameter analyzer. Air annealing of WSe_2 devices was performed by heating WSe_2 devices on a hot plate under a lab environment at different temperatures (50–400 °C) for 1 h. As control experiments, vacuum annealing was performed in a tube furnace at 200 °C for 1 h at a pressure of 12 mTorr. The field-effect mobility of WSe_2 FETs was calculated using the following equation:

$$\mu = \frac{L}{W}\frac{1}{C_{ox}V_{ds}}\frac{dI_{ds}}{dV_g}$$

where L and W are the channel length and width of the FET, respectively. V_{ds} is the source–drain voltage. I_{ds} is the current flowing from source to drain, and V_g is the gate voltage. C_{ox} is the gate capacitance per unit area.

ASSOCIATED CONTENT

Supporting Information

The Supporting Information is available free of charge on the ACS Publications website at DOI: 10.1021/acsnano.6b00527.

Additional AFM, Raman, PL, optical microscopy, and device measurement results (PDF)

AUTHOR INFORMATION

Corresponding Author

*E-mail: chongwuz@usc.edu.

Author Contributions

†B.L. and Y.M. contributed equally.

Notes

The authors declare no competing financial interest.

ACKNOWLEDGMENTS

The authors acknowledge Keji Lai and Di Wu of UT Austin for helpful discussions. This work was supported by the Air Force Office of Scientific Research (AFOSR). We would like to acknowledge the collaboration of this research with King Abdulaziz City for Science and Technology (KACST) *via* the Center of Excellence for Nanotechnologies (CEGN).

REFERENCES

(1) Geim, A. K.; Grigorieva, I. V. Van der Waals Heterostructures. *Nature* **2013**, *499*, 419–425.

(2) Gong, Y.; Lin, J.; Wang, X.; Shi, G.; Lei, S.; Lin, Z.; Zou, X.; Ye, G.; Vajtai, R.; Yakobson, B. I.; Terrones, H.; Terrones, M.; Tay, B. K.; Lou, J.; Pantelides, S. T.; Liu, Z.; Zhou, W.; Ajayan, P. M. Vertical and In-Plane Heterostructures from WS_2/MoS_2 Monolayers. *Nat. Mater.* **2014**, *13*, 1135–1142.

(3) Jariwala, D.; Sangwan, V. K.; Lauhon, L. J.; Marks, T. J.; Hersam, M. C. Emerging Device Applications for Semiconducting Two-Dimensional Transition Metal Dichalcogenides. *ACS Nano* **2014**, *8*, 1102–1120.

(4) Najmaei, S.; Liu, Z.; Zhou, W.; Zou, X. L.; Shi, G.; Lei, S. D.; Yakobson, B. I.; Idrobo, J. C.; Ajayan, P. M.; Lou, J. Vapour Phase Growth and Grain Boundary Structure of Molybdenum Disulphide Atomic Layers. *Nat. Mater.* **2013**, *12*, 754–759.

(5) Xia, F.; Wang, H.; Xiao, D.; Dubey, M.; Ramasubramaniam, A. Two-Dimensional Material Nanophotonics. *Nat. Photonics* **2014**, *8*, 899–907.

(6) Gong, Y.; Liu, Z.; Lupini, A. R.; Shi, G.; Lin, J.; Najmaei, S.; Lin, Z.; Elias, A. L.; Berkdemir, A.; You, G.; Terrones, H.; Terrones, M.; Vajtai, R.; Pantelides, S. T.; Pennycook, S. J.; Lou, J.; Zhou, W.; Ajayan, P. M. Band Gap Engineering and Layer-by-Layer Mapping of Selenium-Doped Molybdenum Disulfide. *Nano Lett.* **2014**, *14*, 442–449.

(7) Liu, Z.; Amani, M.; Najmaei, S.; Xu, Q.; Zou, X.; Zhou, W.; Yu, T.; Qiu, C.; Birdwell, A. G.; Crowne, F. J.; Vajtai, R.; Yakobson, B. I.; Xia, Z.; Dubey, M.; Ajayan, P. M.; Lou, J. Strain and Structure Heterogeneity in MoS_2 Atomic Layers Grown by Chemical Vapour Deposition. *Nat. Commun.* **2014**, *5*, 5246.

(8) Gao, Y.; Liu, Z.; Sun, D. M.; Huang, L.; Ma, L. P.; Yin, L. C.; Ma, T.; Zhang, Z.; Ma, X. L.; Peng, L. M.; Cheng, H. M.; Ren, W. Large-Area Synthesis of High-Quality and Uniform Monolayer WS_2 on Reusable Au Foils. *Nat. Commun.* **2015**, *6*, 8569.

(9) Ji, Q. Q.; Zhang, Y. F.; Gao, T.; Zhang, Y.; Ma, D. L.; Liu, M. X.; Chen, Y. B.; Qiao, X. F.; Tan, P. H.; Kan, M.; Feng, J.; Sun, Q.; Liu, Z. F. Epitaxial Monolayer MoS_2 on Mica with Novel Photoluminescence. *Nano Lett.* **2013**, *13*, 3870–3877.

(10) Zhang, Y.; Zhang, Y. F.; Ji, Q. Q.; Ju, J.; Yuan, H. T.; Shi, J. P.; Gao, T.; Ma, D. L.; Liu, M. X.; Chen, Y. B.; Song, X. J.; Hwang, H. Y.; Cui, Y.; Liu, Z. F. Controlled Growth of High-Quality Monolayer WS_2 Layers on Sapphire and Imaging Its Grain Boundary. *ACS Nano* **2013**, *7*, 8963–8971.

(11) Ling, X.; Lee, Y. H.; Lin, Y. X.; Fang, W. J.; Yu, L. L.; Dresselhaus, M.; Kong, J. Role of the Seeding Promoter in MoS_2 Growth by Chemical Vapor Deposition. *Nano Lett.* **2014**, *14*, 464–472.

(12) Lee, Y. H.; Yu, L. L.; Wang, H.; Fang, W. J.; Ling, X.; Shi, Y. M.; Lin, C. T.; Huang, J. K.; Chang, M. T.; Chang, C. S.; Dresselhaus, M.; Palacios, T.; Li, L. J.; Kong, J. Synthesis and Transfer of Single-Layer Transition Metal Disulfides on Diverse Surfaces. *Nano Lett.* **2013**, *13*, 1852–1857.

(13) Zhan, Y. J.; Liu, Z.; Najmaei, S.; Ajayan, P. M.; Lou, J. Large-Area Vapor-Phase Growth and Characterization of MoS_2 Atomic Layers on a SiO_2 Substrate. *Small* **2012**, *8*, 966–971.

(14) Keum, D. H.; Cho, S.; Kim, J. H.; Choe, D.-H.; Sung, H.-J.; Kan, M.; Kang, H.; Hwang, J.-Y.; Kim, S. W.; Yang, H.; Chang, K. J.; Lee, Y. H. Bandgap Opening in Few-Layered Monoclinic $MoTe_2$. *Nat. Phys.* **2015**, *11*, 482–486.

(15) Li, H. L.; Duan, X. D.; Wu, X. P.; Zhuang, X. J.; Zhou, H.; Zhang, Q. L.; Zhu, X. L.; Hu, W.; Ren, P. Y.; Guo, P. F.; Ma, L.; Fan, X. P.; Wang, X. X.; Xu, J. Y.; Pan, A. L.; Duan, X. F. Growth of Alloy $MoS_{2x}Se_{2(1-x)}$ Nanosheets with Fully Tunable Chemical Compositions and Optical Properties. *J. Am. Chem. Soc.* **2014**, *136*, 3756–3759.

(16) Fang, H.; Chuang, S.; Chang, T. C.; Takei, K.; Takahashi, T.; Javey, A. High-Performance Single Layered WSe_2 p-FETs with Chemically Doped Contacts. *Nano Lett.* **2012**, *12*, 3788–3792.

(17) Huang, J. K.; Pu, J.; Hsu, C. L.; Chiu, M. H.; Juang, Z. Y.; Chang, Y. H.; Chang, W. H.; Iwasa, Y.; Takenobu, T.; Li, L. J. Large-Area Synthesis of Highly Crystalline WSe_2 Mono layers and Device Applications. *ACS Nano* **2014**, *8*, 923–930.

DOI: 10.1021/acsnano.6b00527
ACS Nano XXXX, XXX, XXX–XXX

(18) Liu, W.; Kang, J.; Sarkar, D.; Khatami, Y.; Jena, D.; Banerjee, K. Role of Metal Contacts in Designing High-Performance Monolayer n-Type WSe_2 Field Effect Transistors. *Nano Lett.* **2013**, *13*, 1983−1990.
(19) Liu, B. L.; Fathi, M.; Chen, L.; Abbas, A.; Ma, Y. Q.; Zhou, C. W. Chemical Vapor Deposition Growth of Monolayer WSe_2 with Tunable Device Characteristics and Growth Mechanism Study. *ACS Nano* **2015**, *9*, 6119−6127.
(20) Wang, X. S.; Feng, H. B.; Wu, Y. M.; Jiao, L. Y. Controlled Synthesis of Highly Crystalline MoS_2 Flakes by Chemical Vapor Deposition. *J. Am. Chem. Soc.* **2013**, *135*, 5304−5307.
(21) Mak, K. F.; He, K. L.; Shan, J.; Heinz, T. F. Control of Valley Polarization in Monolayer MoS_2 by Optical Helicity. *Nat. Nanotechnol.* **2012**, *7*, 494−498.
(22) You, Y.; Zhang, X.-X.; Berkelbach, T. C.; Hybertsen, M. S.; Reichman, D. R.; Heinz, T. F. Observation of Biexcitons in Monolayer WSe_2. *Nat. Phys.* **2015**, *11*, 477−481.
(23) Duan, X.; Wang, C.; Shaw, J. C.; Cheng, R.; Chen, Y.; Li, H.; Wu, X.; Tang, Y.; Zhang, Q.; Pan, A.; Jiang, J.; Yu, R.; Huang, Y.; Duan, X. Lateral Epitaxial Growth of Two-Dimensional Layered Semiconductor Heterojunctions. *Nat. Nanotechnol.* **2014**, *9*, 1024−1030.
(24) Xie, J. F.; Zhang, J. J.; Li, S.; Grote, F.; Zhang, X. D.; Zhang, H.; Wang, R. X.; Lei, Y.; Pan, B. C.; Xie, Y. Controllable Disorder Engineering in Oxygen-Incorporated MoS_2 Ultrathin Nanosheets for Efficient Hydrogen Evolution. *J. Am. Chem. Soc.* **2013**, *135*, 17881−17888.
(25) Li, H.; Yin, Z. Y.; He, Q. Y.; Li, H.; Huang, X.; Lu, G.; Fam, D. W. H.; Tok, A. I. Y.; Zhang, Q.; Zhang, H. Fabrication of Single- and Multilayer MoS_2 Film-Based Field-Effect Transistors for Sensing NO at Room Temperature. *Small* **2012**, *8*, 63−67.
(26) Late, D. J.; Huang, Y. K.; Liu, B.; Acharya, J.; Shirodkar, S. N.; Luo, J. J.; Yan, A.; Charles, D.; Waghmare, U.; Dravid, V. P.; Rao, C. N. R. Sensing Behavior of Atomically Thin-Layered MoS_2 Transistors. *ACS Nano* **2013**, *7*, 4879−4891.
(27) Liu, B. L.; Chen, L.; Liu, G.; Abbas, A. N.; Fathi, M.; Zhou, C. W. High-Performance Chemical Sensing Using Schottky-Contacted Chemical Vapor Deposition Grown Mono layer MoS_2 Transistors. *ACS Nano* **2014**, *8*, 5304−5314.
(28) Liu, B.; Köpf, M.; Abbas, A.; Wang, X.; Guo, Q.; Jia, Y.; Xia, F.; Weihrich, R.; Bachhuber, F.; Pielnhofer, F.; Wang, H.; Dhall, R.; Cronin, S. B.; Ge, M. Y.; Fang, X.; Nilges, T.; Zhou, C. W. Black Arsenic-Phosphorus: Layered Anisotropic Infrared Semiconductors with Highly Tunable Compositions and Properties. *Adv. Mater.* **2015**, *27*, 4423−4429.
(29) Lu, J.; Carvalho, A.; Chan, X. K.; Liu, H.; Liu, B.; Tok, E. S.; Loh, K. P.; Castro Neto, A. H.; Sow, C. H. Atomic Healing of Defects in Transition Metal Dichalcogenides. *Nano Lett.* **2015**, *15*, 3524−3532.
(30) Liu, Y.; Tan, C.; Chou, H.; Nayak, A.; Wu, D.; Ghosh, R.; Chang, H. Y.; Hao, Y.; Wang, X.; Kim, J. S.; Piner, R.; Ruoff, R. S.; Akinwande, D.; Lai, K. Thermal Oxidation of WSe_2 Nanosheets Adhered on SiO_2/Si Substrates. *Nano Lett.* **2015**, *15*, 4979−4984.
(31) Balendhran, S.; Deng, J. K.; Ou, J. Z.; Walia, S.; Scott, J.; Tang, J. S.; Wang, K. L.; Field, M. R.; Russo, S.; Zhuiykov, S.; Strano, M. S.; Medhekar, N.; Sriram, S.; Bhaskaran, M.; Kalantar-Zadeh, K. Enhanced Charge Carrier Mobility in Two-Dimensional High Dielectric Molybdenum Oxide. *Adv. Mater.* **2013**, *25*, 109−114.
(32) Yamamoto, M.; Dutta, S.; Aikawa, S.; Nakaharai, S.; Wakabayashi, K.; Fuhrer, M. S.; Ueno, K.; Tsukagoshi, K. Self-Limiting Layer-by-Layer Oxidation of Atomically Thin WSe_2. *Nano Lett.* **2015**, *15*, 2067−2073.
(33) Han, G. H.; Kybert, N. J.; Naylor, C. H.; Lee, B. S.; Ping, J. L.; Park, J. H.; Kang, J.; Lee, S. Y.; Lee, Y. H.; Agarwal, R.; Johnson, A. T. C. Seeded Growth of Highly Crystalline Molybdenum Disulphide Monolayers at Controlled Locations. *Nat. Commun.* **2015**, *6*, 6128.
(34) Kang, K.; Xie, S.; Huang, L.; Han, Y.; Huang, P. Y.; Mak, K. F.; Kim, C. J.; Muller, D.; Park, J. High-Mobility Three-Atom-Thick Semiconducting Films with Wafer-Scale Homogeneity. *Nature* **2015**, *520*, 656−660.
(35) Ma, Y. Q.; Liu, B. L.; Zhang, A. Y.; Chen, L.; Fathi, M.; Shen, C. F.; Abbas, A.; Ge, M. Y.; Mecklenburg, M.; Zhou, C. W. Reversible Semiconducting to Metallic Phase Transition in Chemical Vapor Deposition Grown Monolayer WSe_2 and Applications for Devices. *ACS Nano* **2015**, *9*, 7383−7391.
(36) Zhou, H.; Wang, C.; Shaw, J. C.; Cheng, R.; Chen, Y.; Huang, X.; Liu, Y.; Weiss, N. O.; Lin, Z.; Huang, Y.; Duan, X. Large Area Growth and Electrical Properties of p-Type WSe_2 Atomic Layers. *Nano Lett.* **2015**, *15*, 709−713.
(37) http://srdata.nist.gov/xps/ (Accessed Jan 10, 2016).
(38) Kalantar-zadeh, K.; Vijayaraghavan, A.; Ham, M.-H.; Zheng, H.; Breedon, M.; Strano, M. S. Synthesis of Atomically Thin WO_3 Sheets from Hydrated Tungsten Trioxide. *Chem. Mater.* **2010**, *22*, 5660−5666.
(39) Wu, J.; Li, H.; Yin, Z.; Li, H.; Liu, J.; Cao, X.; Zhang, Q.; Zhang, H. Layer Thinning and Etching of Mechanically Exfoliated MoS_2 Nanosheets by Thermal Annealing in Air. *Small* **2013**, *9*, 3314−3319.
(40) Song, S. H.; Kim, B. H.; Choe, D. H.; Kim, J.; Kim, D. C.; Lee, D. J.; Kim, J. M.; Chang, K. J.; Jeon, S. Bandgap Widening of Phase Quilted, 2D MoS_2 by Oxidative Intercalation. *Adv. Mater.* **2015**, *27*, 3152−3158.

DOI: 10.1021/acsnano.6b00527
ACS Nano XXXX, XXX, XXX−XXX